

# An experimental investigation of convective heat transfer from the heated floor of a rectangular duct to a low frequency, large tidal displacement oscillatory flow

W. L. COOPER, V. W. NEE and K. T. YANG

Thermal Packaging Laboratory, Department of Aerospace and Mechanical Engineering, University of Notre Dame, Notre Dame, IN 46556, U.S.A.

(Received 2 December 1992 and in final form 27 August 1993)

**Abstract**—This research experimentally investigates convective heat transfer from a heated floor section of a rectangular duct to a low frequency, large tidal displacement, oscillatory flow. Phase correlated oscillatory flow velocity and temperature profiles are presented. Favorable pressure gradients, with respect to time, are shown to stabilize the flow while adverse pressure gradients are shown to sustain velocity fluctuations. Higher heat transfer rates are obtained for smaller duct heights, higher oscillation frequencies, and larger tidal displacements. A nondimensional correlation based on a new correlation parameter has been obtained for the oscillatory-flow Nusselt number.

## 1. INTRODUCTION

SIGNIFICANT advances in electronic component miniaturization and processing capabilities have coupled over the past several decades to yield steadily increasing component heat fluxes and densities. These conditions have forced many electronic system designers to adopt direct and indirect liquid and conduction thermal management schemes rather than air-based schemes. Such schemes offer higher heat transfer coefficients at the expense of higher initial costs and maintenance complications [1–8]. Much of the additional expense and complications could be avoided if high enough heat transfer coefficients are available from a practical air-based thermal management system. This paper addresses convective heat transfer to low frequency, large tidal displacement, purely oscillatory flows as a possible method of practically obtaining high heat transfer coefficients.

To the knowledge of the authors, no papers have been published dealing strictly with heat transfer to oscillatory flows. Most related papers discuss heat transfer to modulated flows (oscillatory flows superimposed on mean steady flows) [9–12], and many of these further distance themselves from the present research by considering cases of resonant fluid modulations [13–17]. The latter articles typically deal with heat transfer in pulse combustor tailpipes. That subject has received considerable attention since the introduction of pulse combustor residential heaters by Lennox in the early 1980s [18]. Other articles in the latter category deal with heat transfer enhancement of flow over furrowed or grooved walls by flow modulation. These articles deal with separation structure enhancement via flow modulation [19–26]. The closest related

study from the first group [27] deals with heat transfer from a uniformly heated flat plate in modulated flow. It presents relationships for maximizing the heat transfer augmentation due to the flow modulations. However, the relationships do not hold true in the limit as the mean steady velocity goes to zero. Thus, no prior research exists to link modulated flow phenomena with the oscillatory flow phenomena.

The state of the literature on oscillatory flows, leads the present research to address the heat transfer and fluid mechanics problems simultaneously to yield insight into how oscillatory flows transfer heat. This is done by measuring heat transfer coefficients and phase correlated velocity and temperature profiles. For more information on oscillatory and modulated flow research, see refs. [28, 29].

## 2. EXPERIMENTAL FACILITY

A specially designed oscillatory flow wind tunnel was constructed to experimentally examine heat transfer into rectangular ducts containing an oscillatory flow. The facility design was optimized to reduce external flow disturbances and measurement uncertainty, see Fig. 1(a). The facility is built around a large square (38.1 cm × 38.1 cm) piston and variable height test section (1.905, 3.81, 5.702, 7.595 cm high and 15.24 cm wide). The piston is driven by a one horsepower DC electric motor with variable speed capability. The motor is geared down (10:1) to provide flow oscillation frequencies from 0 to 0.7 Hz (test frequencies include 0.1, 0.15, 0.2, 0.3, 0.4, 0.41, 0.575, 0.6 Hz). A linkage is provided between the radius arm (attached to the motor speed reducer) and the piston arm to create a sinusoidal piston motion. The piston

## NOMENCLATURE

$d$	one-half the duct height [m]	$U_c$	flow centerline velocity [ $\text{m s}^{-1}$ ]
$f$	oscillation frequency [Hz]	$u_x$	uncertainty in parameter $x$
$h$	convective heat transfer coefficient [ $\text{W m}^{-2} \text{K}^{-1}$ ]	$x$	distance along lower wall of test duct [cm]
$k$	thermal conductivity [ $\text{W m}^{-2} \text{K}^{-1}$ ]	$y$	distance from wall [cm].
$l$	heater length [cm]	Greek symbols	
$Nu$	Nusselt number	$\alpha$	Womersley number, $d\sqrt{(\omega/\nu)}$
$q''$	heat flux [ $\text{W m}^{-2}$ ]	$\beta$	oscillatory flow transition number, $\Delta x\sqrt{(\omega/\nu)}$
$Re_{\text{r.m.s.}}$	oscillating flow Reynolds number based on cross-stream averaged r.m.s. velocity and duct height	$\Delta x$	fluid tidal displacement = one-half the flow cross-section averaged distance a fluid particle would move in a complete oscillation cycle if constrained to an infinitely long test section [m]
$Re_{\text{max}}$	maximum oscillatory Reynolds number based on cross-section averaged velocity	$\delta$	Stokes boundary layer thickness, $\sqrt{(2\nu/\omega)}$
$Re_{\omega}$	oscillatory Reynolds number, $2\pi f\Delta x 2d/\nu$	$\eta$	nondimensionalized distance from wall, $y\sqrt{(U_c/\nu x)}$
$S$	stroke length = tidal displacement of piston [m]	$\nu$	kinematic viscosity [ $\text{m}^2 \text{s}^{-1}$ ]
$T$	local fluid temperature [ $^{\circ}\text{C}$ ]	$\omega$	flow oscillation angular frequency [ $\text{rad s}^{-1}$ ].
$T_{1,2}$	temperatures measured by thermocouples 1 and 2 on the surface of the sensor sandwich [ $^{\circ}\text{C}$ ]		
$T_a$	ambient fluid temperature [ $^{\circ}\text{C}$ ]		
$U$	flow velocity [ $\text{m s}^{-1}$ ]		

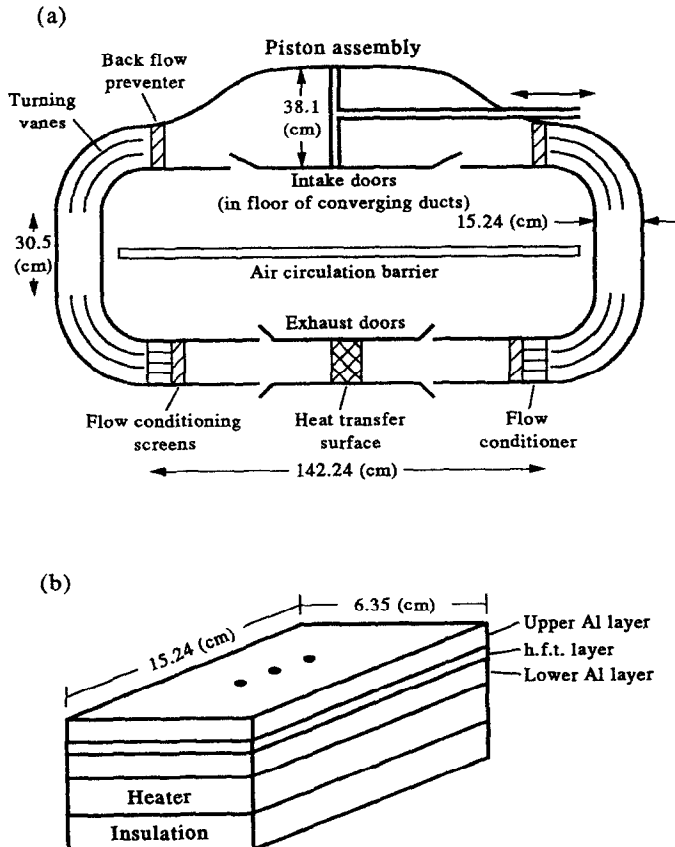


FIG. 1. (a) Oscillatory flow heat transfer facility schematic and (b) sensor sandwich schematic with heater.

head tidal displacement (stroke) is variable from 11.43 to 22.86 cm in increments of 1.27 cm (test strokes include 11.43, 13.97, 15.24, 16.51, 19.05, 20.32, 21.59, and 22.86 cm). A wire wound potentiometer is connected to the output shaft of the speed reducer to correlate measurements in the test duct to the position of the piston head. Thus, temperatures, velocities, etc can be correlated together from separate readings according to their position (from 0 to 360°) in the oscillatory flow cycle. The piston reverses direction at 0, 180 and 360°. It is obvious that 0 and 360° are at the same position, one cycle apart.

Provisions were made (gravity and air pressure driven intake doors, back flow preventers, turning vanes in the 90° bends, flow straighteners, and electronically controlled exhaust doors) to provide fresh air every half oscillation cycle. These ensure that the heat transfer reference temperature is equal to the ambient temperature and prevents air temperature rise in the facility from cycle to cycle. The latter point proved critical because the facility required three hours to reach a thermal cyclic steady state. The test facility uses aluminum doors mounted in the piston chamber floor on either side of the piston head. The piston drives air into the test section by pushing it around the 180° bends. As the piston pushes the air in one direction, a vacuum is created on the other side of the piston head. The back flow preventers do not allow air in the 180° bends to re-enter the piston chamber. Thereby, the intake door is opened and the chamber is filled with air. The doors are lightly weighted so that they close immediately when the piston reverses direction. Seals around the doors' edges prevented leakage.

The backflow preventers are constructed from 2.5 cm high, hinged aluminum strips which span the duct. They are sealed along the edges and allowed to swing in only one direction, thus preventing flow in the other. Two equally spaced, vertical turning vanes are included in each of the 90° bends to guide the air and produce a more uniform flow. The flow straighteners include four screens (0.159 cm mesh openings, separated by 0.635 cm) and a 5 cm long bank of 0.318 cm diameter plastic tubes. The screens help reduce the size of any eddies produced by the 180° bends and the straw bundles help orient the flow parallel to the test section.

The exhaust doors are controlled by electronic solenoids and swing shut parallel to the flow rather than closing like standard doors. This design minimized flow disturbance. The solenoids are triggered by a roller switch and cam assembly on the motor speed reducer. They open and close when the piston reverses direction. The doors alternate positions each half cycle so that the doors downstream of the test section are always open.

A 6.35 cm × 15.24 cm heated floor segment is flush-mounted in the test section for convective heat transfer measurements. It is composed of a three-layer sensor sandwich attached to an electric strip heater

(see Fig. 1(b)). The top and bottom layers are 0.635 cm thick aluminum plates and the middle layer contains a 1.27 cm × 6.35 cm heat flux transducer to measure one dimensional heat flux through the device. An electric strip heater (220 V, 500 W maximum power) is attached to the bottom of the lower aluminum surface to supply the heat flux. The long 15.24 cm side is oriented perpendicular to the flow in the 15.24 cm wide test section.

The upper layer has three type-T thermocouples located near the center of its surface as shown by the three dots in Fig. 1(b). These measure the surface temperature of the upper layer. This plate is mounted on top of the heat flux transducer (h.f.t.) layer to absorb any non-linear temperature gradients induced by the oscillatory flow. This keeps the h.f.t. free from temperature gradient oscillations which could corrupt its measurements. A lumped capacitance analysis of the upper 1.6 mm of the aluminum upper layer indicated that temperature fluctuations on the order of the noise of the data acquisition system could be expected on the upper surface. Test results corroborate this conclusion.

The thermocouple in the center is the primary thermocouple. The other two are included to document the two-dimensionality of the measurements taken. Experimental data indicate that the surface temperature is uniform in the area encompassing the three thermocouples. The thermocouples are flush mounted along the surface to avoid artificially tripping the flow. The upper surface is polished to reduce its emissivity. Radiation losses were estimated to be less than 0.0258 W in<sup>-2</sup> under normal operating conditions. The 1.27 cm × 6.35 cm h.f.t. is centered under the thermocouples so that only the heat flux in the vicinity of the thermocouples is measured. The lower aluminum plate is included to even out any heat flux nonuniformities produced by the strip heater. A partition, between the piston and the test section, and a large fan (which circulated the room air) prevented air from circulating directly from the exhaust to intake doors.

A Disa type 55M01 main unit was used with a type 55M10 standard bridge for constant temperature anemometer (hot wire) flow velocity measurements. The same type main unit with a type 55M20 temperature bridge was used for cold wire flow temperature measurements. Both units used the same Dantek boundary layer type 55P05 wire probe. The cold wire flow temperature measurements were experimentally verified to be independent of the flow velocity. The probe position in the oscillatory flow facility test duct is controlled by a traverse with a position resolution of ±0.013 cm. All measurements were performed in a vertical line over the center of the heated floor section. The heater was not in use during the flow velocity measurements.

Measurement data were acquired using a computer-based 16 bit analog-to-digital converter. See Section 4 for a description of system resolutions and measure-

ment uncertainties. All probe leads and the isothermal junction box were shielded with multiple layers of aluminum foil and grounded. This greatly reduced emf's induced in the probe leads by ambient electromagnetic noise.

### 3. EXPERIMENTAL PROCEDURE

The convective heat transfer coefficients are calculated from the average values of 2160 (72 measurements per flow cycle over 30 cycles) heat flux, surface temperature, and ambient temperature measurements. The measurements were obtained using the 'sensor sandwich' in the floor of the test duct and an ambient temperature thermocouple located near the air intake doors.

The flow velocity was measured at 14 (small duct height) or 16 (larger duct heights) probe locations. The probe locations encompassed one-half of the test duct height, from 0.25 mm from the wall to the flow centerline. Due to the right angle, boundary layer probe mount used, only the flow velocities measured during one-half of the oscillatory flow cycle are accurate. During the other half of the cycle the flow encounters the probe mount prior to the probe. The flow is not heated for any of the velocity measurements. Temperatures were measured in the same manner as the velocities except that the heater was used in all tests and measurements were only made over 20 oscillation cycles.

The system required three hours to reach thermal cyclic steady state for all temperature and heat transfer tests. The flow reached such steady state immediately for the velocity measurements. The term 'cyclic steady state' used here is relative to oscillatory flows and implies that the drift of phase-correlated average measurement values is on the order of the noise of the data acquisition system.

### 4. UNCERTAINTY ANALYSIS

Two main sources of uncertainty exist in the present experiment. These are the calibration uncertainty (which is a function of the accuracy of the calibration standard) and the measurement uncertainty (which is a function of the data acquisition system). See Table 1 for a complete list of measurement uncertainty data. The second and third columns list the signal gains and resulting measurement resolution. The measurement resolution corresponds with the base A/D digital discretization unit associated with each sensor type. The latter value is determined from the input voltage range, signal gain, and number of A/D bits (16).

All probes (with the exception of the h.f.t. which was calibrated at the factory to  $\pm 2\%$ ) were calibrated at a number of points in the expected input range

using 3000 measurements taken over a 12.5 s interval for each point. The mean values were used to construct calibration curves. Column 4 of Table 1 lists the uncertainties of the calibration standards. Due to the dynamic nature of the oscillatory flow, repeated measurements were not possible. Thus, the calibration data were reprocessed to predict the measurement uncertainties (90% and 95% confidence level) associated with any single measurement. The 90% and 95% confidence level single measurement uncertainties are shown in columns 5 and 6 of Table 1. The last column is a r.m.s. combination of columns 3 and 6 (and several other sensor specific uncertainties of which space limitations here preclude the discussion [28]). The listed values are the expected uncertainty in any single measurement quoted at a 95% confidence level.

The velocity and temperature graphs (as a function of piston position) presented later are composed of 2160 (72 measurements per cycle over 30 cycles) or 1440 (72 measurements per cycle over 20 cycles) points, respectively. Because any given measurement point is not repeated, the uncertainty of any one data point is given in the last column of Table 1.

The uncertainty in the convective heat transfer coefficient was calculated using the Kline-McClintock method yielding:

$$u_h = \frac{1}{T_1 + T_2 - 2T_x} \sqrt{((2(T_1 + T_2 - 2T_x)u_q)')^2 + (2q''u_{T_1})^2 + (2q''u_{T_2})^2 + (4q''u_{T_x})^2} \quad (1)$$

for the uncertainty in  $h$ . Averaging the component values (such as  $T_1$ ,  $T_2$ , etc.) substantially reduce the uncertainty in the final result. For example the equation for the average heat flux is:

$$q''_{\text{average}} = \frac{\sum_{i=1}^{2160} q''_i}{2160} \quad (2)$$

The uncertainty in  $q''_{\text{average}}$  is:

$$u_{q''_{\text{average}}} = \sqrt{\left(\sum_{i=1}^{2160} \left(\frac{u_{q''_i}}{2160}\right)^2\right)} \quad (3)$$

Given a typical value of  $q''$  like  $1500 \text{ W m}^{-2}$  and an uncertainty in  $q''$  of  $\pm 2\%$  or  $\pm 30 \text{ W m}^{-2}$ , the uncertainty in the average heat flux is only  $0.6455 \text{ W m}^{-2}$ . The uncertainties in the temperatures are computed similarly resulting in  $u_{T_{\text{average}}} = 0.031^\circ\text{C}$ . Thus, a typical heat transfer coefficient uncertainty is  $\approx \pm 3.26 \text{ W m}^{-2} \text{ K}^{-1}$ , where  $T_1 = T_2 = 60^\circ\text{C}$ ,  $T_x = 22^\circ\text{C}$ , and  $q'' = 1500 \text{ W m}^{-2}$ . This is approximately 12% of the magnitude of typical  $h$  values. Table 2 includes a list of the uncertainties associated with the various heat transfer coefficients.

Table 1. Measurement uncertainty data

Sensor type	Signal gain	A/D converter resolution	Calibration uncertainty	90% confidence	95% confidence	Single measurement uncertainties 95% confidence
Type-T surface thermocouple	500	305 nV or 0.0072°C	±0.1°C	±0.857°C	±1.40°C	±1.434°C
Type-T ambient thermocouple	500	305 nV or 0.0072°C	±0.1°C	±0.913°C	±1.45°C	±1.434°C
Heat flux transducer	10	15.3 μV or 8.35 W m <sup>-2</sup>	±2%	±8.34 W m <sup>-2</sup>	±10.82 W m <sup>-2</sup>	±2%
Potentiometer	1	153 μV or 0.011°	±0.522°	±0.877°	±0.999°	±1.127°
Hot wire	1	153 μV or 0.0068 m s <sup>-1</sup>	±0.053 m s <sup>-1</sup>	±0.00197 m s <sup>-1</sup>	±0.00215 m s <sup>-1</sup>	±0.053 m s <sup>-1</sup>
Cold wire	1	153 μV or 0.0039°C	±0.201°C	±0.6124°C	±0.685°C	+3–4°C bias ±0.7163°C

Table 2. Test parameter and heat transfer relationships

Duct height 2d [cm]	Piston stroke S [cm]	f [Hz]	Δx [m]	α	β	Re <sub>max</sub>	(l/d)Re <sub>o</sub> <sup>2/3</sup>	h [W m <sup>-2</sup> K <sup>-1</sup> ]	u <sub>n</sub> 95% [W m <sup>-2</sup> K <sup>-1</sup> ]
1.905	16.51	0.3	8.26	3.28	2843	9327	1.70E+10	30.509	2.652
1.905	20.32	0.41	10.16	3.84	4091	15 689	3.71E+10	43.977	3.580
1.905	20.32	0.6	10.16	4.64	4949	22 960	6.56E+10	61.543	4.848
1.905	22.86	0.6	11.43	4.64	5567	25 830	7.83E+10	67.718	5.302
3.81	13.97	0.2	3.49	5.36	982	5262	3.59E+09	17.304	1.842
3.81	13.97	0.4	3.49	7.58	1389	10 523	1.02E+10	23.102	1.278
3.81	15.24	0.4	3.81	7.58	1515	11 480	1.16E+10	25.250	2.311
3.81	22.86	0.575	5.72	9.08	2725	24 753	3.68E+10	41.854	3.430
5.702	16.51	0.15	2.76	6.94	672	4664	2.01E+09	15.411	1.742
5.702	21.59	0.2	3.61	8.02	1014	8132	4.63E+09	17.941	1.877
5.702	15.24	0.6	2.55	13.89	1240	17 220	1.43E+10	26.992	2.422
5.702	15.24	0.4	2.55	11.34	1012	11 480	7.77E+09	21.586	2.086
7.595	13.97	0.3	1.75	13.08	603	7892	3.31E+09	16.861	1.818
7.595	19.05	0.3	2.39	13.08	823	10 762	5.28E+09	18.299	1.897
7.595	21.59	0.3	2.71	13.08	933	12 197	6.38E+09	19.444	1.961

1.75 < Δx < 11.43 m; 3.28 < α < 13.89; 603 < β < 5567.

## 5. RESULTS AND DISCUSSIONS

### 5.1. Heat transfer coefficients

Convective heat transfer coefficients and Nusselt numbers were obtained for a number of test parameter groups. Table 2 lists the relationship between the various test parameter combinations and the tidal displacement, Womersley number ( $\alpha$ ), transition number ( $\beta$ ),  $Re_{\max}$ ,  $(l/d)Re_o^{2/3}$ , and convective heat transfer coefficient. The Nusselt number is merely  $hl/k_{\text{air}}$  where  $l$  is the heater length and  $k_{\text{air}}$  is the conductivity of air. The test parameter combinations were chosen to yield a distribution of Womersley and transition numbers in the range under consideration. The maximum and minimum values are listed at the bottom of Table 2.

The flow tidal displacement is one-half the cross-stream averaged distance a fluid particle would move in an infinitely long test section during one complete flow oscillation cycle. The dimensionless Womersley number ( $\alpha$ ) is the same as the classical Stokes number and is equal to  $\alpha = d\sqrt{(2\pi f/\nu)}$  where  $d$  is one-half the

duct height,  $f$  is the oscillation frequency, and  $\nu$  is the kinematic viscosity. Typically  $d$  is the tube radius when cylindrical geometries are considered. The Womersley number is the ratio of the viscous diffusion time scale to the oscillation time scale. As such, it measures the propagation of viscously conveyed flow information relative to the rate at which the flow characteristics change. Typically, low Womersley number flows are laminar. The dimensionless transition number is similar,  $\beta = \Delta x\sqrt{(2\pi f/\nu)}$ , differing only by the inclusion of the tidal displacement rather than the duct half-height. The transition number is referred to as such because it is used in the literature to denote the regimes where velocity fluctuations (other than the expected global sinusoidal fluctuation) occur during portions of the oscillation cycle. A comparison of the transition number and the peak Reynolds numbers calculated for the different test flows yields an interesting and predictable result. See Table 2. The transition numbers which correspond to oscillatory flow transition (approximately 400–700) also

correspond with transitional peak Reynolds numbers for the rectangular test ducts as shown in Table 2. Prior research has noted that velocity fluctuations (about the expected sinusoidal pattern) are typically associated with the peak flow velocities if they appear in the flow at all. This is related to the fact that the flow is exceeding typical transitional Reynolds numbers during the peak velocity phases of the flow. However, as noted later, the Reynolds number is not a self-sufficient oscillatory flow transition criteria due to the transient nature of the flow.  $Re_{max}$  is the maximum Reynolds number for a given parameter set and is based on the maximum cross-stream averaged velocity. The dimensionless quantity  $(l/d)Re_{\omega}^{3/2}$  is the heat transfer data correlation parameter discussed in the following paragraphs. The last two columns are the convective heat transfer coefficients and their uncertainties quoted at a 95% confidence level, respectively.

The experimental results in terms of the convective heat transfer coefficients and Nusselt numbers show that expectedly higher Nusselt numbers are obtainable for smaller duct heights, higher oscillation frequencies, and larger tidal displacements. However, the Nusselt numbers do not correlate well with the maximum Reynolds number, Womersley number, or the transition number. None of these parameters contain sufficient information on the physical phenomena to collapse all the data. An attempt has been made to find appropriate correlation parameters, and based on the governing differential equations for laminar flow, the scaling laws pertinent to the oscillatory flow phenomenon, Reynolds analogy, and existing results for Stokes flow and duct flows, a correlation parameter [28]

$$\frac{l}{d}Re_{\omega} = \left(\frac{l}{d}\right)\left(\frac{2\pi f\Delta x 2d}{v}\right)^{3/2} \quad (4)$$

has been found to correlate well all the experimental heat transfer data as shown in Fig. 2. Here  $d$  is the

half duct height,  $l$  is the heater length in the direction of flow,  $f$  is the flow oscillation frequency,  $v$  is the kinematic viscosity,  $\Delta x$  is the tidal displacement, and  $Re_{\omega}$  is the oscillatory Reynolds number. It is important to realize that the quantity  $(2d\Delta x)$  in the oscillatory Reynolds number is directly proportional to the piston volume, which is a constant in the present study, and consequently  $Re_{\omega}$  is really only a function of the frequency for the data obtained here.

The data presented in Fig. 2 clearly show two limiting behaviors of heat transfer, as represented by the two linear lines in the log-log plot. We term the limit as the duct height becomes large as the large-gap limit characterized by relatively small Nusselt numbers, while the other limit is known as the small-gap limit with ever increasing Nusselt numbers. There is also a relatively small transition region bridging the two limits. Obviously these limiting regions can also be interpreted as the contrasting Reynolds number regimes for fixed duct height. As will be shown and discussed in the following sections, these limiting behaviors are associated with distinctly different flow phenomena.

5.2. Flow velocities

Flow velocities were examined as a function of piston position at 14 (smallest duct height) or 16 locations (larger duct heights) spanning 0.25 mm from the wall to the centerline of the test duct. Seven different test parameter groups (chosen from those listed in Table 2) were tested to establish the similarity of flows under different test conditions. Typical raw CTA data at a single probe location appears as shown in Fig. 3 where 2160 points are included. Test points were acquired 72 times per oscillation cycle over 30 cycles at each probe location. The points between 0 and 180° do not represent the true velocity of the flow. During that portion of the cycle the flow encounters the hot wire probe mount prior to the probe. This alters the velocity that the probe sees. These points are included

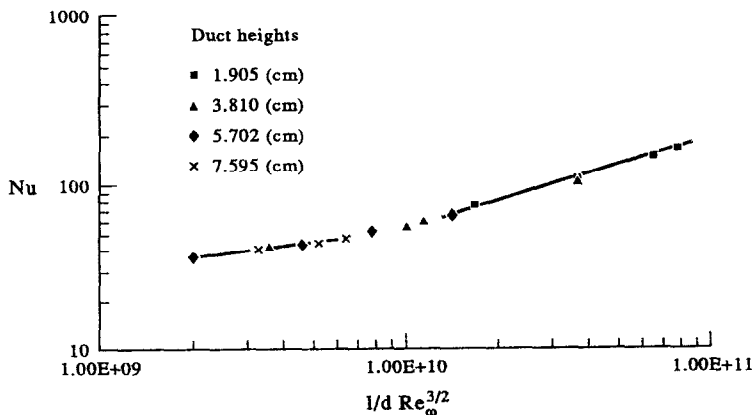


FIG. 2. Nusselt number correlation.

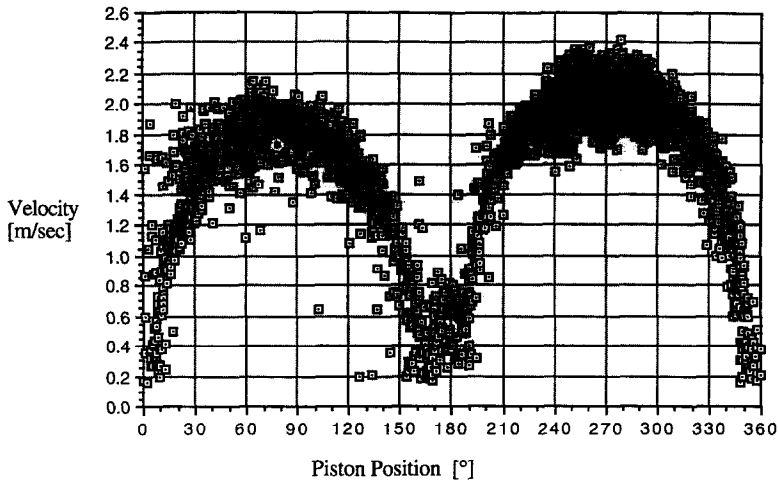


FIG. 3. Flow velocity vs piston position with  $S = 15.24$  cm,  $d = 1.905$  cm,  $f = 0.4$  Hz, 2.502 mm from wall.

to show the phase relationship between the flow and the piston position. The dark lines which appear in the test points approximate the most common (not necessarily the mean) velocity profile with respect to different probe positions. The lines are created by high point densities. Vertical scatter in the points indicates deviation of the velocity profile from the most common (dark) path from one cycle to the next. This is indicative of flow velocity fluctuations and departures from laminar flow. The clusters of test points around  $180^\circ$  and  $360^\circ$  (or  $0^\circ$ ) are due to the opening and closing of the exhaust doors along the test duct.

All flow velocity (and temperature) measurements were made along a single vertical line over the center of the heat flux transducer assembly. No measurements were performed to determine the spatial development of the oscillatory flow velocity profiles. The heater attached to the heat flux transducer assembly was not on during any of the velocity measurements.

Note that the points maintain a tight grouping as the flow accelerates ( $190^\circ$ – $210^\circ$ ) and then spread out as the flow reaches peak velocity. The favorable pressure gradient (with respect to time) which exists during flow acceleration dampens flow disturbances and relaminarizes the flow. This occurs despite the presence of velocity fluctuations just prior to flow reversal. The point grouping loosens up as the flow approaches its peak Reynolds number. The flow maintains its loose point grouping from the region of highest Reynolds number ( $270^\circ$ ) until the flow reverses direction again ( $360^\circ$ ). This is due to the presence of an adverse pressure gradient (with respect to time) which decelerates the flow and sustains flow disturbances. The disturbances shown near  $180^\circ$  and  $360^\circ$  are due primarily to the opening and closing of the exhaust doors near the test section. These disturbances have little effect on the flow, thanks to the relaminarization effect.

The transient nature of the flow and the relaminarization effect combined to reduce the sig-

nificance of the Reynolds number in predicting flow transition. The transition number is commonly used in the literature to predict the onset of velocity fluctuations about the global sinusoidal oscillation. However, no study has conclusively differentiated between velocity fluctuations and actual flow turbulence. It is questionable whether the flow is ever fully developed during any part of the oscillatory cycle. Thus, the use of conventional transition criteria is questionable also. This is an aspect of oscillatory flow research which needs further attention.

The velocity fluctuations denoted by the point scatter in Fig. 3 (i.e. lack of phase-correlated velocity repetition from cycle to cycle) are found primarily in the shear layer next to the wall. Figure 4(a) shows the velocity profiles and various flow layers associated with low Reynolds number oscillatory flows (the left-hand linear region in Fig. 2). The flow can be divided into three main layers. The inner layer next to the wall is dominated by viscous effects (Stokes layer). The outer layer is characterized by an inviscid slug flow character (inviscid layer). The layer in between the wall and the inviscid layer is dominated by the ambient, time varying pressure gradient (shear layer). Figure 4(b) shows the depth of the Stokes layer relative to the half-width of a high Reynolds number oscillatory flow (the right-hand linear region in Fig. 2). The shear layer in this case extends across the entire flow. Thus, although the velocity fluctuations are larger near the wall, they can be expected everywhere in the flow. The phase-correlated velocity profiles shown in Figs. 4(a) and (b) are constructed by averaging the raw CTA data (like that shown in Fig. 3) at each probe location over multiple  $20^\circ$  piston position ranges. For instance, the data associated with the  $230^\circ$  velocity profile in Fig. 4(a) are constructed by averaging points in the range  $220^\circ$ – $240^\circ$ . Data from  $260^\circ$  to  $010^\circ$  are used to construct the velocity profiles from  $90^\circ$  to  $170^\circ$  because the data from  $0^\circ$  to  $180^\circ$  are

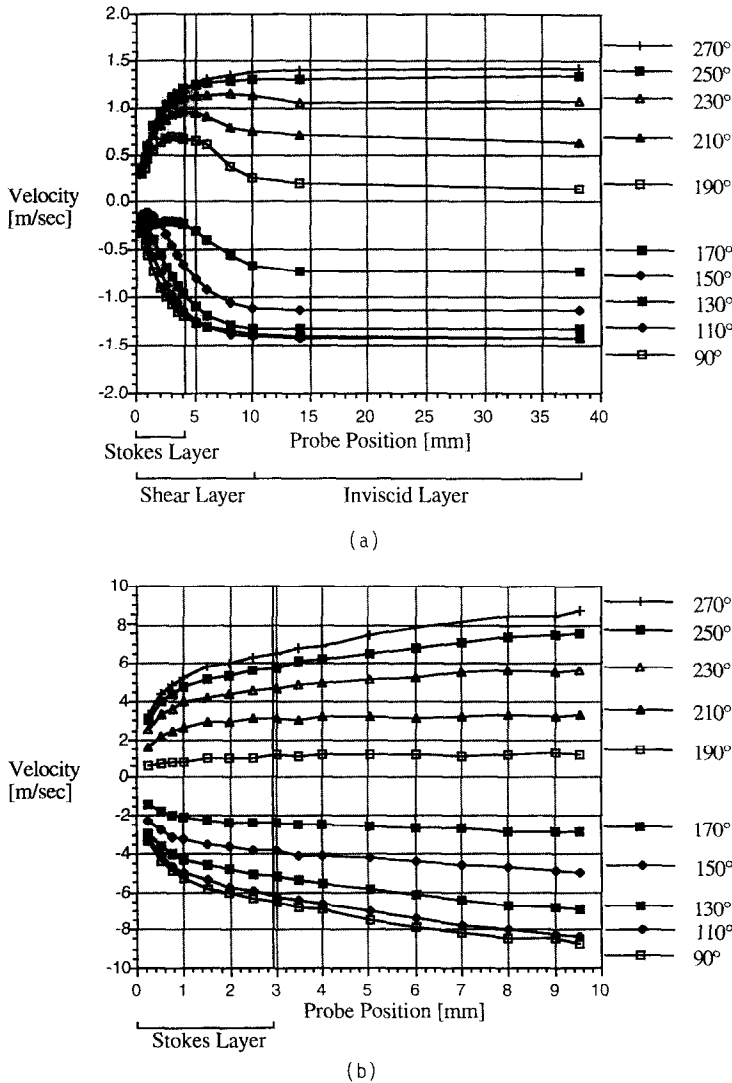


FIG. 4. (a) Phase correlated, direction compensated velocity profiles with  $S = 11.43$  cm,  $d = 3.798$  cm,  $f = 0.3$  Hz and (b) phase correlated, direction compensated velocity profiles with  $S = 22.86$  cm,  $d = 0.953$  cm,  $f = 0.6$  Hz.

corrupted by the probe mount. During that portion of the flow cycle the flow encounters the probe mount prior to the probe. All the velocity profiles are a compilation of data taken over thirty cycles because the raw data was acquired over thirty oscillation cycles.

The positions in the oscillation cycle at which the flow reverses direction typically do not correspond with the 180 and 360° positions at which the piston reverses direction and the doors along the test duct are actuated. The fluid flowing closest to the wall reverses direction first and the flow in the center of the duct reverses last. The flow reverses as much as 35–40° sooner in the shear layer than along the centerline of the flow. This phenomenon can be seen in Fig. 4(a). Note that as the flow in the inviscid layer approaches a zero velocity, the flow in the shear layer has already reversed. Such flow reversal effects appear

typical of Stokes flows and are primarily a function of the varying pressure gradient. All seven data sets tested exhibit this behavior. Similar effects have been noted in modulated flow research [30–34] and in the inlet contractions of pipes, where static or pumped pressure heads accelerate the fluid from rest into pipe inlets. The key difference in the inlet contraction case is that the developing velocity profile in a pipe inlet is comparable to the initial, transient half-oscillation cycle which does not involve flow reversal from the previous half cycle.

The reason for the two distinct linear regions in Fig. 2 can be most clearly seen in Figs. 4(a) and (b). The left-hand linear region, or the large-gap limit, of Fig. 2 is characterized by lower Reynolds numbers and the separate viscous and inviscid layers shown in Fig. 4(a). The flow Reynolds numbers are low by virtue

of the large duct heights. Increasing the duct height decreases the flow velocity and the Reynolds number for a given piston volume. The duct heights are large enough that the shear layers near the upper and lower walls are separated by an inviscid layer. The inviscid layer prevents the shear layers from interacting, resulting in shear layer velocity profiles predictable by the classic Stokes flow velocity solution. The shear layers are dominated by the time-varying pressure gradient, and significant velocity fluctuations are limited to the shear layer. Little or no fluid is exchanged between the shear layers and the inviscid layer. The resulting flow mixing and heat transfer is thereby limited to the shear layers near the walls. The right-hand linear region of Fig. 2, or the small-gap limit, is characterized by higher Reynolds numbers and a shear layer that spans the entire duct. Thus, the velocity fluctuations in the shear layer are found throughout the flow. In this manner the entire flow is involved in flow mixing and heat transfer. The result is an increase in slope of the Nusselt numbers shown in Fig. 2.

Figure 5 shows several phase-correlated velocity profiles non-dimensionalized in the standard Blasius profile fashion. Prior to nondimensionalization the data were prepared like those in Figs. 4(a) and (b). A standard laminar (Blasius) profile is included for comparison. The parameter  $\eta$  is defined as:  $\eta = y\sqrt{(U_c/\nu x)}$  where  $y$  is the distance from the wall,  $U_c$  is the centerline velocity,  $\nu$  is the kinematic viscosity, and  $x$  is approximated as 0.508 m (the length of the test section floor from the flow straightener to the center of the heat flux transducer assembly). All the sets of test parameters but one exhibit boundary layer profiles fuller than the Blasius profile as shown

in Fig. 5. This equates to much larger velocity gradients local to the wall (true for all test sets). The largest velocity gradients and the fullest velocity profiles occur at the beginning of the flow acceleration phase (180–200°). The velocity profiles approach the Blasius profile as the oscillation cycle continues through the acceleration phase and then into the deceleration phase. The significance of this trend is that the wall to free stream diffusion distance is reduced by up to 70% relative to steady laminar flows.

### 5.3. Flow temperature profiles

Figure 6(a) displays a typical raw set of temperature measurement data. Again, the dark lines in the figure represent the most common temperature profile with respect to piston position. The temperature peaks at 180 and 360° arise because the flow is momentarily stopped while reversing at those positions. Lower flow temperatures generally correspond with higher flow velocities. When the flow velocity is low, the ratio of the heat diffusion time relative to the flow time of residence over the heated plate is low. Increasing that ratio results in lower flow temperatures. The construction of Fig. 6(a) is similar to Fig. 3 except that measurements were only acquired over twenty flow cycles.

The phase of the temperature profiles relative to the piston position does not change significantly with changes in the probe position, i.e. the minimum flow temperatures occur at about 90 and 270° and the maximum flow temperatures occur at about 0 (or 360) and 180°. This is in contrast to the velocity profiles which change phase relative to piston position (based on position of flow reversal).

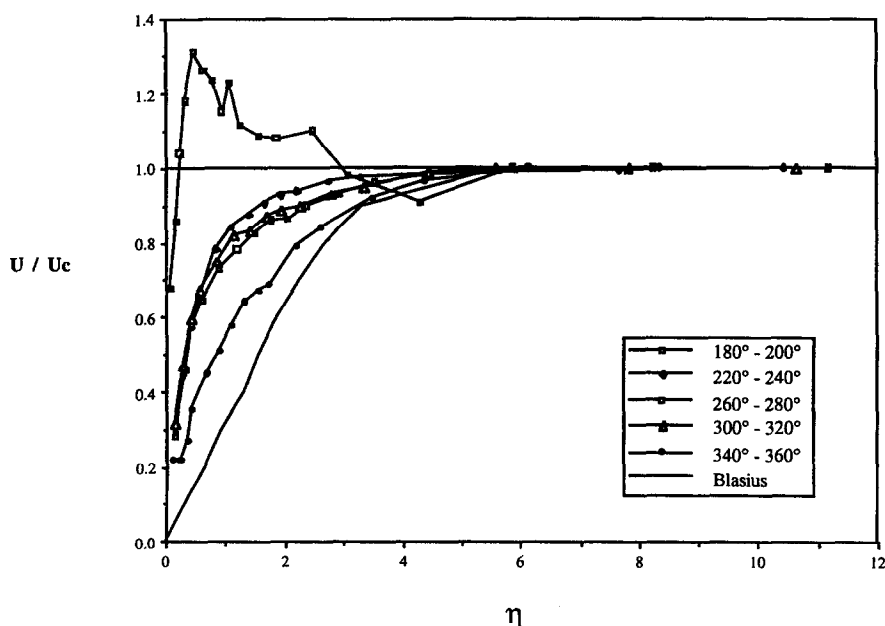


FIG. 5. Normalized phase correlated velocity profiles with  $S = 15.24$  cm,  $d = 1.905$  cm,  $f = 0.4$  Hz.

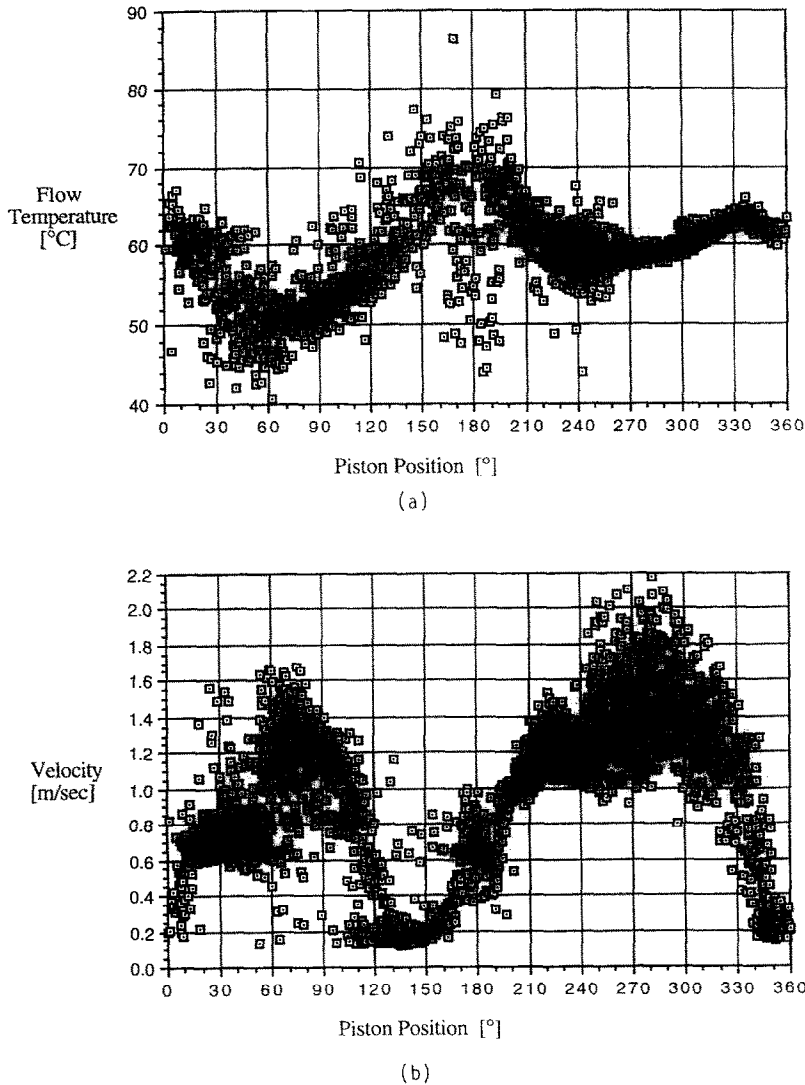


FIG. 6. (a) Fluid temperature vs piston position with  $S = 15.24$  cm,  $d = 1.905$  cm,  $f = 0.4$  Hz, 0.749 mm from wall, and (b) flow velocity vs piston position with  $S = 15.24$  cm,  $d = 1.905$  cm,  $f = 0.4$  Hz, 0.749 mm from wall.

During the 180–360° portion of the oscillation cycle in Figs. 6(a) and (b), note the correlation between scatter in the velocity data and the lack of scatter in the temperature data, and vice versa. The scatter in the velocity data is indicative of flow mixing which creates a repeatable, well mixed temperature pattern. The lack of scatter in the velocity data indicates a lack of flow mixing. During such phases the flow temperature falls prey to spurious velocity fluctuations or fluid buoyancy effects which do not mix the flow well and scatter the temperature data.

Figure 7 shows typical phase correlated temperature profiles. The profiles were constructed using the same method used in Figs. 4(a) and (b) to construct the velocity profiles. The temperature gradients local to the wall are greatest when the flow velocity is maximum, i.e. when the piston position is approxi-

mately 240–300° (or 60–120°). Heat diffusion causes a greater temperature increase in the flow while the flow is reversing than when the flow is at its peak Reynolds number. This follows from the diffusion to residence time ratio. When the flow is slow or stopped, the residence time is high, allowing more heat per unit of volumetric flow to diffuse. This results in higher flow temperatures and less steep temperature gradients. The steeper gradients arise also due to increased flow mixing near the peak flow Reynolds numbers.

## 6. CONCLUSIONS

(1) It was found that the oscillatory flow Nusselt number depends on a single dimensionless parameter  $(l/d)Re_w^{3/2}$  and that the correlation exhibits a large-

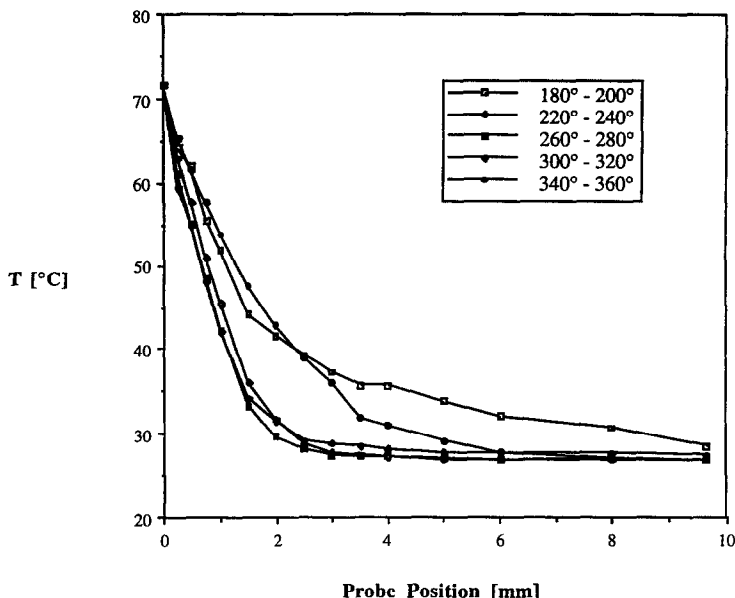


FIG. 7. Phase correlated temperature profiles with  $S = 16.5$  cm,  $d = 0.953$  cm,  $f = 0.3$  Hz.

gap limit and a small-gap limit, as a result of the diminishing of the inviscid center layer.

(2) Accelerating or favorable pressure gradients (with respect to time) are stabilizing and dampen velocity fluctuations. Decelerating or adverse pressure gradients are destabilizing and sustain flow fluctuations.

(3) Prior research has not conclusively linked the velocity fluctuations found in oscillatory flows with the presence of turbulence. The presence of a time-varying pressure gradient alters the flow and even produces a relaminarization effect during flow acceleration. Thus, using the transition number or maximum Reynolds number criterias can only, at best, predict the onset of significant velocity fluctuations.

(4) Measured flow temperature fluctuations in the shear layer behave opposite to the velocity fluctuations. When velocity fluctuations are present, the flow is well mixed, and a repeatable temperature pattern is obtained and vice versa.

(5) The non-dimensionalized velocity gradients near the heat transfer surface are greater for the oscillatory flows tested than for steady laminar flows. Therefore, the oscillatory flow velocity profiles are fuller than the laminar Blasius profile.

*Acknowledgement*—The authors would like to acknowledge the financial support from the IBM Corporation, Endicott, New York.

#### REFERENCES

1. A. E. Bergles, The evolution of cooling technology for electrical, electronic, and microelectronic equipment, *Heat Transfer in Electronic Equipment, ASME HTD* **57**, 1-11 (1986).
2. O. Folberth, The interdependence of geometrical, thermal, and electrical limitations for VLSI logic, *IEEE J. Solid-State Circuits* **1**, 51-53 (1981).
3. B. Hoeneisen and C. Mead, Fundamental limits in microelectronics technology—I. MOS technology, *Solid State Electronics* **15**, 819-829 (1972).
4. J. Kaye, Review of industrial applications of heat transfer in electronics, Research Laboratory of Heat Transfer in Electronics Rept. No. RLHTE-12, Massachusetts Institute of Technology, Cambridge; *Proc. IRE*, Vol. 44, pp. 977-991 (1956).
5. R. Keyes, Fundamental limits in digital signal processing, *Proc. IEEE* **69**(4), 267-278 (1981).
6. W. Nakayama and A. E. Bergles, Cooling electronic equipment: past, present, and future. In *Heat Transfer in Electronic and Microelectronic Equipment* (Edited by A. E. Bergles), pp. 3-60. Hemisphere, Washington, D.C. (1986).
7. C. Seitz and J. Matisoo, Engineering limits on computer performance, *Physics Today* 38-45 (1984).
8. W. Pence and J. Krusius, The fundamental limits for electronic packaging and systems, *IEEE Trans. CHMT* **2**, 176-183 (1987).
9. D. O. Barnett and R. I. Vachon, An analysis of convective heat transfer for pulsating flow in a tube, *Proc. 4th Int. Heat Transfer Conf.* (1970).
10. F. J. Bayley, P. A. Edwards and P. P. Singh, The effect of flow pulsations on heat transfer by forced convection from a flat plate, *Int. Heat Transfer Conf.*, August, Boulder, Colorado (1961).
11. D. W. Bogandoff, A study of the mechanisms of heat transfer in oscillatory flow, Technical Report no. 483-f, October, Princeton University (1967).
12. V. Chalithbhan, Effect of longitudinal oscillations in heat transfer, Ph.D. Thesis, University of Texas, January (1959).
13. A. A. Alhaddad and G. A. Coulman, Experimental and theoretical study of heat transfer in pulse-combustion heaters, *Proc. 1, Symp. on Pulse Combust. Appl.*, GRI-82/0009.2, Atlanta, Georgia, March (1982).

14. J. E. Dec and J. O. Keller, Pulse combustor tail-pipe heat-transfer dependence on frequency, amplitude, and mean flow rate, *Combust. Flame* **77**, 359–374 (1989).
15. B. M. Galitseiskii, A. A. Nozdrin, Yu. A. Ryzhov and E. V. Yakush, Investigation of local heat-transfer coefficient under conditions of the resonance oscillations of a gas in channels, *J. Engng Phys.* **31**(2), 873–876 (1976).
16. P. C. Lalwani, K. L. Das, T. K. Bhattacharyya and D. Bhaduri, Heat transfer characteristics of a pulsating combustion system, *Mech. Engng Bull.* **10**(3–6), 7–10 (1979).
17. E. H. Perry and F. E. C. Culick, Measurements of wall heat transfer in the presence of large-amplitude combustion driven oscillations, *Combust. Sci. Technol.* **9**, 49–53 (1974).
18. A. A. Putnam, F. E. Belles and J. A. C. Kentfield, Pulse combustion, *Prog. Energy Combust. Sci.* **12**, 43–79 (1986).
19. J. S. Nigen and C. H. Amon, Forced convection cooling enhancement of surface-mounted electronic package configurations through self-sustained oscillatory flows, *ASME HTD* **171**, 39–46 (1991).
20. N. K. Ghaddar, K. Z. Korczak, B. B. Mikic and A. T. Patera, Numerical investigation of incompressible flow in grooved channels. Part 1. Stability and self-sustained oscillations, *J. Fluid Mech.* **163**, 99–127 (1986).
21. N. K. Ghaddar, M. Magen, B. B. Mikic and A. T. Patera, Numerical investigation of incompressible flow in grooved channels. Part 2. Resonance and oscillatory heat transfer enhancement, *J. Fluid Mech.* **168**, 541–567 (1986).
22. M. Greiner, N. K. Ghaddar, B. B. Mikic and A. T. Patera, Resonant convective heat transfer in grooved channels, *Proceedings of the 8th International Heat Transfer Conference*, Vol. 6, pp. 2867–2872 (1986).
23. A. T. Patera and B. B. Mikic, Exploiting hydrodynamic instabilities. Resonant heat transfer enhancement, *Int. J. Heat Mass Transfer* **29**(8), 1127–1138 (1986).
24. I. J. Sobey, On flow through furrowed channels. Part 1. Calculated flow patterns, *J. Fluid Mech.* **96**(1), 1–26 (1980).
25. I. J. Sobey, Oscillatory flows at intermediate Strouhal number in asymmetric channels, *J. Fluid Mech.* **125**, 359–373 (1982).
26. K. D. Stephanoff, I. J. Sobey and B. J. Bellhouse, On flow through furrowed channels. Part 2. Observed flow patterns, *J. Fluid Mech.* **96**, 27–32 (1980).
27. N. Fujita and T. Tsubouchi, An experimental study of unsteady heat transfer from a flat plate to an oscillatory air flow, *Heat Transfer—Jap. Res.* **11**(3), 31–43 (1982).
28. W. L. Cooper, An experimental investigation of convective heat transfer from the heated floor of a rectangular duct into a low frequency large tidal displacement oscillating flow, M.S. Thesis, Department of Aerospace and Mechanical Engineering, University of Notre Dame, September (1992).
29. W. L. Cooper, K. T. Yang and V. W. Nee, Fluid mechanics of oscillatory and modulated flows and associated applications in heat and mass transfer—a review, *J. Energy, Heat Mass Transfer* **15**, 1–19 (1993).
30. J. E. Dec, J. O. Keller and I. Hongo, Time-resolved velocities and turbulence in the oscillating flow of a pulse combustor tail pipe, *Combust. Flame* **83**, 271–292 (1991). Also Sandia National Laboratories Report. SAND88-8844.
31. S. C. Ling and H. B. Atabek, A nonlinear analysis of pulsatile flow in arteries, *J. Fluid Mech.* **55**, 493–511 (1972).
32. L. Shemer, I. Wygnanski and E. Kit, Pulsating flow in a pipe, *J. Fluid Mech.* **153**, 313–337 (1985).
33. B. R. Ramaprian and S.-W. Tu, An experimental study of oscillatory pipe flow at transitional Reynolds numbers, *J. Fluid Mech.* **100**(3), 513–544 (1980).
34. M. Hino, M. Sawamoto and S. Takasu, Experiments on transition to turbulence in an oscillatory pipe flow, *J. Fluid Mech.* **75**, 193–207 (1976).